Progress In Electromagnetics Research, PIER 100, 309–325, 2010

SENSITIVITY ANALYSIS OF 3-D COMPOSITE STRUCTURES THROUGH LINEAR EMBEDDING VIA GREEN'S OPERATORS

V. Lancellotti, B. P. De Hon, and A. G. Tijhuis

Department of Electrical Engineering
Eindhoven University of Technology
P. O. Box 513, 5600 MB Eindhoven, The Netherlands

Abstract—We propose a methodology — based on linear embedding via Green's operators (LEGO) and the eigencurrent expansion method (EEM) — for solving electromagnetic problems involving large 3-D structures comprised of $N_D \gg 1$ bodies. In particular, we address the circumstance when the electromagnetic properties or the shape of one body differ from those of the others. In real-life structures such a situation may be either the result of a thoughtful design process or the unwanted outcome of fabrication tolerances. In order to assess the sensitivity of physical observables to localized deviations from the "ideal" structure, we follow a deterministic approach, i.e., we allow for a finite number of different realizations of one of the bodies. Then, for each realization we formulate the problem with LEGO and we employ the EEM to determine the contribution of the $N_D - 1$ "fixed" bodies. Since the latter has to be computed *only once*, the overall procedure is indeed efficient. As an example of application, we investigate the sensitivity of a 2-layer array of split-ring resonators with respect to the shape and the offset of one element in the array.

1. INTRODUCTION

Among the numerical techniques that over the past decades have been devised for solving large electromagnetic (EM) problems, the fast multipole method (FMM) [1] along with its multi-level (MLFMA) extension [2] plays a prominent role. Both FMM and MLFMA provide a recipe to perform fast matrix-vector multiplications: Thereby they are intrinsically suited for an iterative solution of the algebraic systems

Corresponding author: V. Lancellotti (v.lancellotti@tue.nl).

arising from the application of the Method of Moments (MoM) [3, 4]. However, when multiple sources are contemplated — e.g., as in the calculation of the monostatic radar cross section (RCS) [5] — iterative methods do not seem to be the obvious choice, as the relevant system needs to be solved for every source, possibly leading to long calculation times. As a matter of fact, for a sweep of source positions (or angles of incidence, frequency and the like) the number of right-hand sides — and hence of systems to be solved — may be reduced drastically with the aid of the marching-on techniques [6, 7]. Nevertheless iterative methods may still suffer from slow convergence rates, when the system matrix is poor- or ill-conditioned.

In this scenario, domain decomposition methods (DDM) [8–15] perform far better, chiefly because, upon introducing ad hoc *locally* entire domain basis functions to expand the unknowns, they effectively *compress* the original system matrix. The latter can then be inverted by direct methods, such as the `LU` factorization [16]; hence multiple right hand sides (i.e., multiple sources) can be accounted for very efficiently and convergence problems of the linear system are avoided.

Driven by these considerations, we have recently extended the linear embedding via Green's operators (LEGO) method [17] for dealing with fully 3-D composite structures [18, 19], comprised of $N_D \gg 1$ disjoint bodies. LEGO is a DDM in which the multiple scattering between adjacent objects is determined through the interaction of simply-shaped building *bricks* (Fig. 1), whose EM

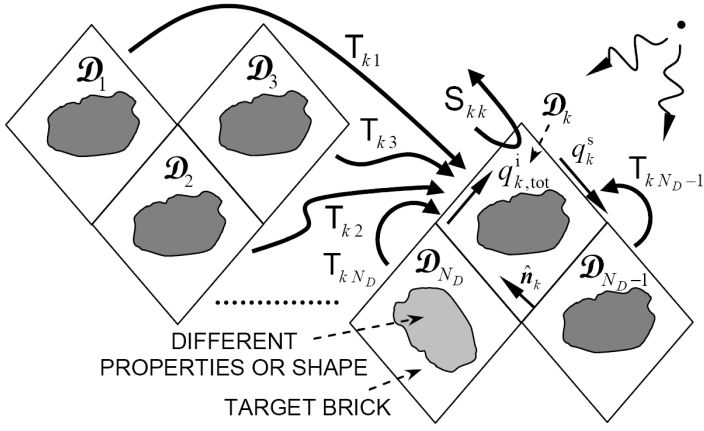

Figure 1. LEGO method: An aggregate of N_D bodies is modelled with as many bricks described via scattering operators S_{kk} (1), whereas the interactions among the bricks are expressed through transfer operators T_{kn} (3). Possible local non-uniformities are included within the N_Dth brick.

behavior is accounted for by means of *scattering operators*.

Here we report on a further upgrade of LEGO to the instance when *one* of the bodies forming the structure is different from the other $N_D - 1$. For such a problem, we have devised a methodology hinging on the following three main steps:

(i) We embed the objects in N_D bricks with identical shape; the brick enclosing the different body is referred to as the "target", whereas the remaining $N_D - 1$ bricks constitute the large "fixed" part of the structure.

(ii) We solve for the large fixed part *once for all* by means of the eigencurrent expansion method (EEM) [18–20].

(iii) We invert a comparatively small linear system for determining the contribution of the target.

The idea of isolating a body with different properties within a target brick was applied in the 2-D LEGO as well [17]. Yet, in [17], we obtained the contribution of the large fixed part of the structure by a cascade of successive embedding steps — which in general is not suited for large 3-D EM problems. The very strategy outlined above was first adopted in [21] to study the properties of an open 3-D electromagnetic band-gap dielectric cavity as a function of the permittivity of the cavity itself. We also followed a similar approach for solving an antenna problem in [22]. Therefore, LEGO stands out as a useful design tool.

On the other hand, one may as well be interested in assessing the performance of an otherwise regular arrangement of objects (e.g., an antenna array) when one of the constitutive elements is "defective". To carry out the sensitivity analysis in such a case, we propose a deterministic approach, namely, we allow for a finite number of possible defective configurations (with respect to the expected one) of one object in the structure. Then, for each configuration we solve the EM problem with LEGO, as outlined above. The procedure turns out convenient, in that, to cope with the defects, we just need to recompute a relatively small matrix (i.e., the scattering operator of the target brick) and invert a system of the same size. Therefore, direct methods may be used, even when $N_D \gg 1$. In contrast, if we were to solve the same problem with MoM and, say, the FMM, then for each realization of the defective object we would have to recompute a substantive part of the whole system matrix. What's more, we would have to repeat the whole iterative solution, as no intermediate result could be reused to save time.

The rest of the paper is organized as follows. We formulate the EM problem in Fig. 1 with LEGO and we solve it by the EEM in Sections 2 and 3, respectively. Then in Section 4, we provide validation of the

numerical code against the baseline MoM and we discuss the sensitivity of the transmission efficiency of a 2-layer array of split-ring resonators (SRR) versus the shape and offset of one defective element in the array. A time dependence in the form $\exp(\mathrm{j}\omega t)$ for EM fields and sources is implied and suppressed throughout.

2. FORMULATION WITH LEGO

We consider the scattering from an aggregate of N_D distinct bodies immersed in a (homogeneous) host medium, as depicted in Fig. 1. To formulate this problem with LEGO, we embed the objects in 3-D (arbitrarily shaped) bounded domains $\mathcal{D}_k$, $k = 1, \ldots, N_D$, which we dub *bricks*: We assume that all of the bricks possess the same shape. Besides, we allow one of the bodies to be different (either in shape or in composition) and we enclose it in the N_Dth brick. This is no limitation, since bricks' numbering is irrelevant. Then, we invoke Love's Equivalence Principle [23] to characterize the EM behavior of the bricks — independently of one another and the external sources — by means of scattering operators S_{kk} [18], namely,

$$q_k^{\mathrm{s}} = \mathsf{S}_{kk} q_k^{\mathrm{i}}, \tag{1}$$

where $q^{\mathrm{s,i}}$ are defined in [18, Equation (2)]. In words, S_{kk} maps equivalent incident currents q_k^{i} on $\partial\mathcal{D}_k^+$ (reproducing the incident field inside $\mathcal{D}_k$) to equivalent scattered currents q_k^{s} on $\partial\mathcal{D}_k^-$ (radiating the scattered field outside $\mathcal{D}_k$). We obtain S_{kk} by posing proper boundary integral equations (BIEs) on $\partial\mathcal{D}_k$ and the object surface [18]. In accordance with the scenario above, $\mathsf{S}_{N_D N_D}$ will be different from S_{kk}, $k < N_D$.

We now observe that (1) holds true for a *solitary* brick in the host medium. When a structure is modelled by means of N_D interacting bricks, (1) generalizes to [18]

$$q_k^{\mathrm{s}} = \mathsf{S}_{kk} \left(q_k^{\mathrm{i}} + \sum_{n \neq k}^{N_D} q_{k(n)}^{\mathrm{i}} \right) = \mathsf{S}_{kk} q_{k,\mathrm{tot}}^{\mathrm{i}}, \quad \forall k, \tag{2}$$

where we have introduced the total incident currents $q_{k,\mathrm{tot}}^{\mathrm{i}}$. The latter are the sum of two terms. The first, q_k^{i}, is the contribution of the external independent sources, i.e., the same as in (1). The second is the sum of additional incident currents, $q_{k(n)}^{\mathrm{i}}$, which are due to the scattered currents q_n^{s}, $n \neq k$, existing on the boundaries of the remaining $N_D - 1$ bricks (see Fig. 1). Symbolically,

$$q_{k(n)}^{\mathrm{i}} = \mathsf{T}_{kn} q_n^{\mathrm{s}}, \ n \neq k, \tag{3}$$

where T_{kn} denotes the transfer operator from $\partial\mathcal{D}_n^-$ to $\partial\mathcal{D}_k^+$ [18]. To proceed, we recast (2) and (3) as:

$$\mathsf{S}_{\mathrm{LL}}^{-1} q_{\mathrm{L}}^{\mathrm{s}} = q_{\mathrm{L}}^{\mathrm{i}} + \mathsf{T}_{\mathrm{L}N_D} \mathsf{S}_{N_D N_D} q_{N_D,\mathrm{tot}}^{\mathrm{i}}, \tag{4}$$

$$q_{N_D,\mathrm{tot}}^{\mathrm{i}} = q_{N_D}^{\mathrm{i}} + \mathsf{T}_{N_D\mathrm{L}}\, q_{\mathrm{L}}^{\mathrm{s}}, \tag{5}$$

where $q_{\mathrm{L}}^{\mathrm{s,i}}$ are column vectors with entries $(q_{\mathrm{L}}^{\mathrm{s,i}})_k = q_k^{\mathrm{s,i}}$, $k < N_D$, and we have made use of the total inverse scattering operator of the large fixed part, $\mathsf{S}_{\mathrm{LL}}^{-1}$, the total transfer operators from the target to the fixed part, $\mathsf{T}_{\mathrm{L}N_D}$, and vice versa, $\mathsf{T}_{N_D\mathrm{L}}$. Furthermore, $\mathsf{S}_{\mathrm{LL}}^{-1}$, $\mathsf{T}_{\mathrm{L}N_D}$, $\mathsf{T}_{N_D\mathrm{L}}$ are a square matrix, a column vector and a row vector, respectively, with entries that are operators given by:

$$(\mathsf{S}_{\mathrm{LL}}^{-1})_{kn} = \begin{cases} \mathsf{S}_{kk}^{-1} & k = n, \\ -\mathsf{T}_{kn} & k \neq n, \end{cases} \quad k, n < N_D, \tag{6}$$

$$(\mathsf{T}_{\mathrm{L}N_D})_k = \mathsf{T}_{k\,N_D},\ k < N_D, \tag{7}$$

$$(\mathsf{T}_{N_D\mathrm{L}})_n = \mathsf{T}_{N_D\,n},\ n < N_D. \tag{8}$$

In the next section we describe how to perform the numerical solution of (4), (5) efficiently by means of the EEM.

3. SOLUTION WITH EEM

The practical implementation of the EEM reflects the one we described in [18, Section 4]. Yet, since we have to tailor the EEM to the system of coupled Equations (4), (5), we provide a short review of the procedure.

3.1. Overview

The EEM [18, 20] consists of applying the MoM [4] with a set of basis and test functions $\mathbb{E}$ which are "approximations" to the eigenfunctions of the operator to be inverted, viz., $\mathsf{S}_{\mathrm{LL}}^{-1}$. Thereby, we choose the entries of $\mathbb{E}$ to be:

$$e_m^{(k)} = \left[\ 0, \ldots, 0, u_m^{(k)}, 0, \ldots\ \right]^t,\ \ k < N_D,\ \ m \in \mathbb{N}, \tag{9}$$

where $u_m^{(k)}$ denotes the mth eigenfunction of S_{kk}. We call $e_m^{(k)}$ *eigencurrents*. Since the eigencurrent $e_m^{(k)}$ coincides with $u_m^{(k)}$ on $\partial\mathcal{D}_k$ and vanishes on $\partial\mathcal{D}_n$, $n \neq k$, evidently, $\{e_m^{(k)}\}$ would constitute the *exact* eigencurrents of $\mathsf{S}_{\mathrm{LL}}^{-1}$, if we had neglected the multiple scattering occurring among the bricks.

When we do take into account the EM interactions among the bricks, $\{e_m^{(k)}\}$ are nevertheless well suited to represent the unknown

scattered currents $q_{\mathrm{L}}^{\mathrm{s}}$. In fact, $\{e_m^{(k)}\}$ can be separated into two subsets:

- *coupled eigencurrents*: They are associated with the largest eigenvalues of S_{kk}, and substantially depart from the true eigencurrents of $\mathsf{S}_{\mathrm{LL}}^{-1}$, say $s_m^{(k)}$.
- *uncoupled eigencurrents*: They correspond to the higher-order eigenvalues of S_{kk}, and they do not interact with one another, in that they are increasingly better approximations to $s_m^{(k)}$.

In [18, 19, 21], we demonstrated that the entries of the MoM matrices obtained using the eigencurrents as basis and test functions are not equally meaningful. More precisely, we can neglect (i.e., nullify) the entries that arise from the interaction of pairs of coupled and uncoupled eigencurrents or two distinct uncoupled eigencurrents. In Section 3.3, we exploit this property to drastically reduce the size of the matrix $[S_{\mathrm{LL}}]^{-1}$, i.e., the algebraic counterpart of $\mathsf{S}_{\mathrm{LL}}^{-1}$.

3.2. Numerical Setup

To build the set $\mathbb{E}$ in (9) we need the eigencurrents $\{u_m^{(k)}\}$. As in general the latter are not known in closed form, we determine $\mathbb{E}$ numerically through the MoM. To this purpose, we model $\partial\mathcal{D}_k$ with a 3-D triangular-facet mesh, on which we define a set $\mathbb{B}_k$ of $2N_F$ Rao-Wilton-Glisson (RWG) functions [24] to expand the current densities $q_k^{\mathrm{s,i}}$ [18, Equation (20)]. Similarly, we represent each object's boundary, $\mathcal{S}_{\mathrm{o}}$, by a triangular mesh, to which we associate a set $\mathbb{C}_k$ of N_{Ok} RWG functions to expand the currents induced on $\mathcal{S}_{\mathrm{o}}$. As argued in [18], the exact structure of $\mathbb{C}_k$ depends on the nature of the BIE posed on the object. In addition, we allow $\mathbb{C}_{N_D}$ to be different from $\mathbb{C}_k$, $k < N_D$, as the object embedded in the target brick may also have a different shape (see Fig. 1).

To proceed, we apply the MoM (in Galerkin's form) to compute the algebraic counterparts of S_{kk} and T_{kn}, i.e., the scattering and transfer matrices $[S_{kk}]$, $[T_{kn}]$, whose size is $2N_F \times 2N_F$ (we refer the reader to [18] for the details.) Hence, we can write the algebraic (weak) form of (4), (5): The resulting expressions are quite straightforward, so we omit them for the sake of brevity. Instead, we give the algebraic counterpart of the relevant operators, viz.,

$$([S_{\mathrm{LL}}]^{-1})_{kn} = \begin{cases} [S_{kk}]^{-1} & k = n, \\ -[T_{kn}] & k \neq n, \end{cases} \quad k, n < N_D, \tag{10}$$

$$([T_{\mathrm{L}N_D}])_k = [T_{k\,N_D}]\,, \; k < N_D, \tag{11}$$

$$([T_{N_D\mathrm{L}}])_n = [T_{N_D\,n}]\,, \; n < N_D. \tag{12}$$

because these matrices will be *compressed* by the EEM. The total inverse scattering matrix (10) is of size $2N_F(N_D-1)\times 2N_F(N_D-1)$, whereas the sizes of $[T_{\mathrm{L}N_D}]$ and $[T_{N_D\mathrm{L}}]$ are $2N_F(N_D-1)\times 2N_F$ and $2N_F\times 2N_F(N_D-1)$, respectively. We emphasize that in (10) the diagonal blocks of $[S_{\mathrm{LL}}]^{-1}$ have to be interpreted formally, as $[S_{kk}]$ is rank-deficient whenever $2N_F > N_{Ok}$. Nonetheless, we are not in trouble, because we never compute $[S_{kk}]^{-1}$ in practice: We will clarify this point in Section 3.3.

As a third step, we determine the $2N_F$ eigenvectors $[v_p^{(k)}]$ and eigenvalues λ_{pk}, $p=1,\ldots,2N_F$, of $[S_{kk}]$. This spectral decomposition [16, 25] has to be effected only once. Then, out of $[v_p^{(k)}]$ we form a larger basis $\mathbb{U}$ for spanning the space of $[q_{\mathrm{L}}^{\mathrm{s,i}}]$, namely,

$$[V]=\mathrm{diag}\{[V_{kk}]\},\ k<N_D, \tag{13}$$

where $[V_{kk}]$ stores the eigenvectors $[v_p^{(k)}]$ columnwise. Apparently, $\mathbb{U}$ represents the algebraic (finite) counterpart of the basis $\mathbb{E}$ defined in Section 3.1.

Finally, we expand the matrices (10)–(12) in the basis $\mathbb{U}$ by means of the eigencurrent matrix (13), namely,

$$([\tilde{S}_{\mathrm{LL}}]^{-1})_{kn}=\begin{cases}\mathrm{diag}\{\lambda_{pk}^{-1}\}, & k=n,\\ -[\tilde{T}_{kn}], & k\neq n,\end{cases}\quad k,n<N_D, \tag{14}$$

$$[\tilde{T}_{\mathrm{L}N_D}]=[V]^{-1}[T_{\mathrm{L}N_D}],\ [\tilde{T}_{N_D\mathrm{L}}]=[T_{N_D\mathrm{L}}][V], \tag{15}$$

where $[\tilde{T}_{kn}]=[V_{kk}]^{-1}[T_{kn}][V_{nn}]$.

3.3. Matrix Compression

As anticipated in Section 3.1, we now nullify the entries of the matrices in (14), (15), when they involve *either* a pair of coupled and uncoupled eigencurrents *or* two distinct uncoupled eigencurrents. To be specific, upon introducing a permutation matrix $[P]$ ($[P]^{-1}$) [16], whose action consists of swapping columns (rows) of the matrix by which it is right (left) multiplied, we have:

$$[\hat{S}_{\mathrm{LL}}]^{-1}=[P]^{-1}[\tilde{S}_{\mathrm{LL}}]^{-1}[P]=\begin{bmatrix}[\tilde{S}_{\mathrm{CC}}]^{-1} & [\tilde{S}_{\mathrm{CU}}]^{-1}\\ [\tilde{S}_{\mathrm{UC}}]^{-1} & [\tilde{S}_{\mathrm{UU}}]^{-1}\end{bmatrix}\approx\begin{bmatrix}[\tilde{S}_{\mathrm{CC}}]^{-1} & [0]\\ [0] & [\Lambda_{\mathrm{UU}}]^{-1}\end{bmatrix}, \tag{16}$$

$$[\hat{T}_{N_D\mathrm{L}}]=[\tilde{T}_{N_D\mathrm{L}}][P]=\begin{bmatrix}[\tilde{T}_{N_D\mathrm{C}}] & [\tilde{T}_{N_D\mathrm{U}}]\end{bmatrix}\approx\begin{bmatrix}[\tilde{T}_{N_D\mathrm{C}}] & [0]\end{bmatrix}, \tag{17}$$

$$[\hat{T}_{\mathrm{L}N_D}]=[P]^{-1}[\tilde{T}_{\mathrm{L}N_D}]=\begin{bmatrix}[\tilde{T}_{\mathrm{C}N_D}]\\ [\tilde{T}_{\mathrm{U}N_D}]\end{bmatrix}\approx\begin{bmatrix}[\tilde{T}_{\mathrm{C}N_D}]\\ [0]\end{bmatrix}, \tag{18}$$

where $[\Lambda_{\mathrm{UU}}]$ is diagonal and stores the eigenvalues of the uncoupled eigencurrents in $\mathbb{U}$. The subscript C (U) stands for coupled (uncoupled). Thanks to (16)–(18), the algebraic equations to be solved take on the final (reduced) form:

$$([I_{N_D N_D}]-[\Sigma_{N_D N_D}][S_{N_D N_D}])[q^{\mathrm{i}}_{N_D,\mathrm{tot}}]=([q^{\mathrm{i}}_{N_D}]+[\tilde{T}_{\mathrm{C}N_D}][\tilde{S}_{\mathrm{CC}}][\tilde{q}^{\mathrm{i}}_{\mathrm{LC}}]), \tag{19}$$

$$[q^{\mathrm{s}}_{N_D}] = [S_{N_D N_D}]\,[q^{\mathrm{i}}_{N_D,\mathrm{tot}}], \tag{20}$$

$$[\tilde{q}^{\mathrm{s}}_{\mathrm{LC}}] = [\tilde{S}_{\mathrm{CC}}]([\tilde{q}^{\mathrm{i}}_{\mathrm{LC}}] + [\tilde{T}_{\mathrm{C}N_D}][q^{\mathrm{s}}_{N_D}]), \tag{21}$$

$$[\tilde{q}^{\mathrm{s}}_{\mathrm{LU}}] = [\Lambda_{\mathrm{UU}}][\tilde{q}^{\mathrm{i}}_{\mathrm{LU}}], \tag{22}$$

where $[I_{N_D N_D}]$ is the identity matrix over the target brick, $[\Sigma_{N_D N_D}] = [\tilde{T}_{N_D\mathrm{C}}][\tilde{S}_{\mathrm{CC}}][\tilde{T}_{\mathrm{C}N_D}]$, and $[\tilde{q}^{\mathrm{s,i}}_{\mathrm{LC}}]$ ($[\tilde{q}^{\mathrm{s,i}}_{\mathrm{LU}}]$) is a column vector containing the coefficients of all the coupled (uncoupled) eigencurrents. Furthermore, we interpret $[\Sigma_{N_D N_D}]$ as the scattering operator of the fixed part as "seen" from $\partial\mathcal{D}_{N_D}$. Notice that (22) can be solved independently, whereas we can go on to determine $[q^{\mathrm{s}}_{N_D}]$ and $[\tilde{q}^{\mathrm{s}}_{\mathrm{LC}}]$ only after solving (19). As a last step, we obtain the expansion coefficients in the original RWG basis from (21) and (22) through:

$$[q^{\mathrm{s}}_{\mathrm{L}}] = [V]\,[P]\left[\begin{array}{c}[\tilde{q}^{\mathrm{s}}_{\mathrm{LC}}]\\ [\tilde{q}^{\mathrm{s}}_{\mathrm{LU}}]\end{array}\right]. \tag{23}$$

Equations (19)–(22) show that only the coupled eigencurrents participate in the multiple scattering that takes place among the bricks of the fixed part as well as between them and the target.

In addition to the advantages of LEGO/EEM [18, 19], the extension we have described has its own benefits:

(i) The determination of $[\tilde{S}_{\mathrm{CC}}][\tilde{q}^{\mathrm{i}}_{\mathrm{LC}}]$, $[\Sigma_{N_D N_D}]$, $[\tilde{S}_{\mathrm{CC}}][\tilde{T}_{\mathrm{C}N_D}]$ requires formally inverting $[\tilde{S}_{\mathrm{CC}}]^{-1}$ of size $N_C(N_D-1)\times N_C(N_D-1)$. Since, normally, $N_C \ll 2N_F$, $[\tilde{S}_{\mathrm{CC}}]^{-1}$ can be easily stored and the calculations can be carried out through `LU` decomposition and backward substitution [16, 25] only once.

(ii) The system matrix in (19) is the same size as the $[S_{kk}]$ (i.e., comparatively small), thereby the solution can be tackled by means of `LU` decomposition as well. More importantly, to deal with various realizations of the target brick we only have to recompute $[S_{N_D N_D}]$ as many times as necessary, while leaving the rest unchanged.

(iii) The calculation of $[\tilde{q}^{\mathrm{s}}_{\mathrm{LU}}]$ in (22) entails just multiplication by the eigenvalues of the uncoupled eigencurrents. These eigenvalues may be null when $[S_{kk}]$ is rank-deficient ($2N_F > N_{Ok}$) [19], but, since we need not evaluate $[\Lambda_{\mathrm{UU}}]^{-1}$ explicitly in (16), the stability of the EEM is not endangered, as anticipated.

Table 1. Breakdown of computational cost of (19), (21).

Matrix	# operations required
$[\tilde{S}_{\mathrm{CC}}]$	$N_C^3(N_D-1)^3$
$[\tilde{S}_{\mathrm{CC}}][\tilde{T}_{\mathrm{C}N_D}]$	$2N_FN_C^2(N_D-1)^2$
$[\tilde{T}_{N_D\mathrm{C}}][\tilde{S}_{\mathrm{CC}}]$	$2N_FN_C^2(N_D-1)^2$
$[\tilde{T}_{N_D\mathrm{C}}]([\tilde{S}_{\mathrm{CC}}][\tilde{T}_{\mathrm{C}N_D}])$	$(2N_F)^2N_C(N_D-1)$
$[\Sigma_{N_DN_D}][S_{N_DN_D}]$	$(2N_F)^3$
$([I_{N_DN_D}]-[\Sigma_{N_DN_D}][S_{N_DN_D}])^{-1}$	$(2N_F)^3$

As for the complexity of the present LEGO/EEM extension, in Table 1 we list the computational cost relevant to some of the matrix inversions and multiplications involved in (19)–(22). The order of magnitude of the overall cost for solving one realization of the target (at a given frequency) can be estimated on summing the various contributions.

4. VALIDATION AND RESULTS

We have upgraded our numerical code to solve (19)–(22). In [18], we validated LEGO/EEM against the bare MoM by comparing the scattered fields in the Fraunhofer region, whereas in [19] we provided near-field validation and a criterion for choosing the number of coupled eigencurrents. Here we briefly focus on assessing the EEM applied to (4), (5).

To this purpose, we consider the plane wave scattering [$\mathbf{E}^{\mathrm{i}} = 1\hat{\mathbf{y}}\exp(-j\mathbf{k}\cdot\mathbf{r})\,\mathrm{V/m}$, $\mathbf{k} = 2\pi\hat{\boldsymbol{z}}/\lambda_0$] off $N_D = 2$ z-aligned (either PEC or dielectric) spheres with radii a_1, a_2, $a_1 > a_2$, [Fig. 2(a)]; then, in Fig. 2(b) we show the LEGO model involving as many cubic bricks (edge d). We embed the smaller sphere within the target brick, i.e., the upper one in Fig. 2(b). In these numerical tests, $2N_F = 1152$, $N_{O1} = 684$, $N_{O2} = 276$, when the spheres are PEC, whereas $N_{O1} = 1368$, $N_{O2} = 552$, when they are penetrable. We employed $N_C(N_D-1) = 50$ coupled eigencurrents. This number has to be contrasted to the size of $[S_{\mathrm{LL}}]^{-1}$, namely, $2N_F(N_D-1) = 1152$, and to the size of the system that arises from the baseline MoM, $N_{O1}+N_{O2} \in \{960, 1920\}$, when applied to an EFIE and a PMCHWT equation [4], respectively. The latter also constitute our reference solutions.

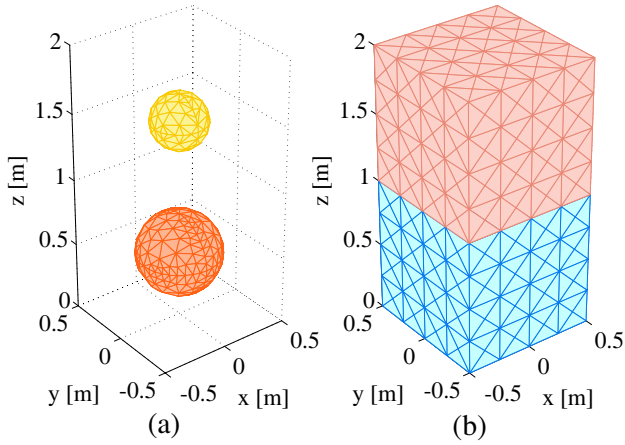

Figure 2. For LEGO/EEM validation: (a) A composite structure consisting of $N_D = 2$ different spheres and (b) the corresponding LEGO model with as many cubic bricks; the top (pink) brick plays the role of the "target".

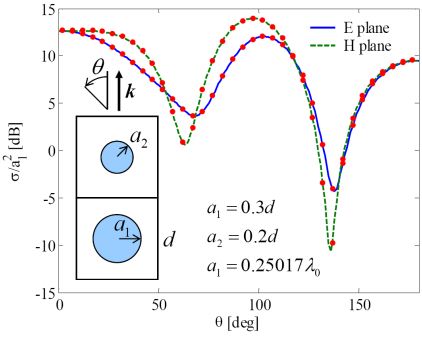

Figure 3. LEGO/EEM validation: bistatic RCS of the structure in Fig. 2 comprised of two PEC spheres. The LEGO/EEM solution (•) with a target brick (and $N_C = 50$) is compared to the MoM solution (–/– –). Insets: sketches of the spheres and the LEGO bricks along with geometrical and physical quantities.

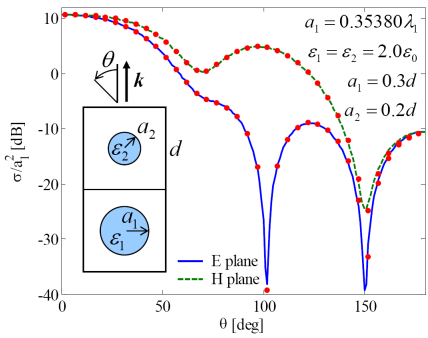

Figure 4. Same as Fig. 3 but for two dielectric spheres.

In Figs. 3 and 4, we report the RCS for the PEC and the dielectric cases, respectively, as well as the relevant geometrical and physical data. The comparisons turn out excellent, thus supporting the validity of the reduced formulation (19)–(22).

As an example of application we consider an array of $N_D = 14 \times 7 \times 2 = 196$ SRRs [13, 26, 27] shown in Fig. 5. The array is immersed in free-space and illuminated by an elemental electric dipole (moment $1\hat{\mathbf{y}}$ Am) placed at $\mathbf{r}_S = (-1.2, 1.7, 1.35)$ mm. Now, suppose that one of the SRRs is "defective" as per either its size or its position with respect to the otherwise regular 3-D rectangular arrangement. The intended SRR and the five defective realizations we considered are shown in Fig. 6. We also allowed (in successive simulation campaigns) for two positions of the defective SRR in the array: These locations are highlighted in Fig. 5 as well. We applied LEGO/EMM with $2N_F = 504$ (see inset of Fig. 5), $N_{Ok} = N_{ON_D} = 446$, $N_C = 30$. Accordingly, the ranks of $[S_{\mathrm{LL}}]^{-1}$ and $[\tilde{S}_{\mathrm{CC}}]^{-1}$ are 98280 and 5850, respectively, whereas the rank of the system matrix in (19) is just 504.

We carried out simulations for 29 frequency samples evenly distributed in the range [90, 104] GHz. Computing q_k^s for one frequency and five realizations of the target roughly required 445 s on a Linux-based x86_64 workstation endowed with an Intel Xeon 2.66-GHz processor and 8-GB RAM. Subsequent calculation of near fields on

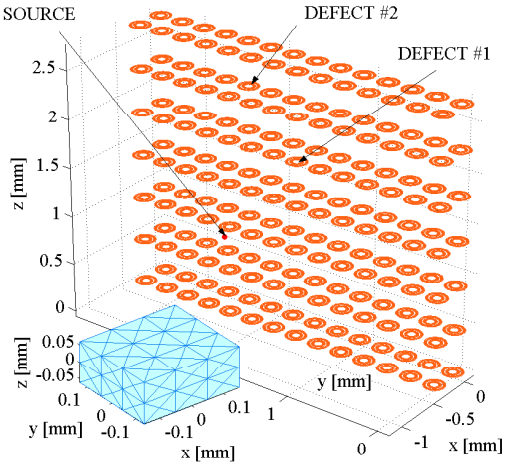

Figure 5. 2-layer array of $N_D = 196$ SRRs illuminated by an electric dipole. Also indicated are the positions of the defective SRRs detailed in Fig. 6. Inset: triangular-facet patching of a LEGO brick enclosing an SRR.

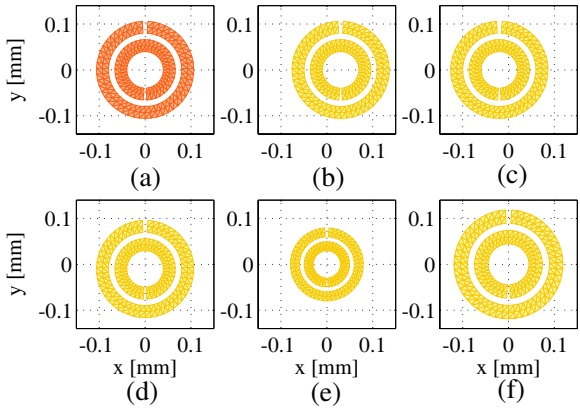

Figure 6. Top view of a SRR and triangular-facet model: (a) Intended size and position, (b) positive $\hat{\mathbf{x}}$-offset, (c) negative $\hat{\mathbf{x}}$-offset, (d) negative $\hat{\mathbf{y}}$-offset, (e) down scaling, (f) up scaling. The axes of the plots coincide with the (xOy trace of the) surrounding LEGO brick (see inset of Fig. 5).

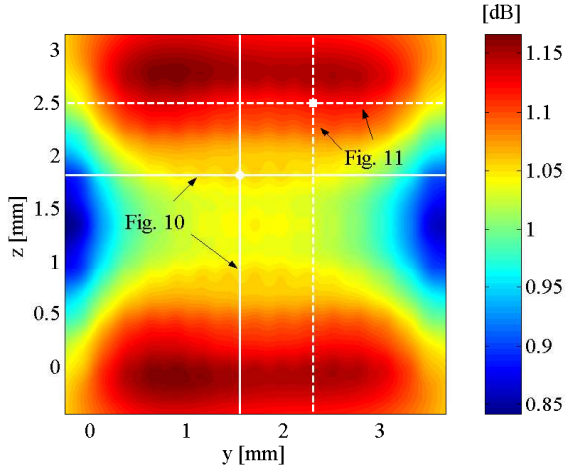

Figure 7. Transmission efficiency (24) of the regular array in Fig. 5 through a planar square surface set in $x = 0.3\,\mathrm{mm}$ at $f = 100\,\mathrm{GHz}$. The markers (•, ■) denote the projection of the defective SRRs as well as the points where $\mathcal{T}$ was computed in Figs. 8 and 9. The continuous (dashed) white straight lines denote the cuts of $\mathcal{T}$ shown in Fig. 10 (Fig. 11).

a square grid of 90×90 observation points in $x = 0.3\,\text{mm}$ (for one frequency and one configuration of the target) took about 741 s. For a more detailed discussion of timing issues in LEGO/EEM, see [18, 21].

Lastly, we computed the transmission efficiency [27], viz.,

$$\mathcal{T}(\mathbf{r}) = \frac{P_{\text{av}}^{\text{tot}}(\mathbf{r})}{P_{\text{av}}^{\text{i}}(\mathbf{r})}, \quad P_{\text{av}}^{\text{i,tot}} = \frac{1}{2}\Re\{\mathbf{E}^{\text{i,tot}} \times (\mathbf{H}^{\text{i,tot}})^*\} \cdot \hat{\mathbf{x}}, \tag{24}$$

and investigated its sensitivity to the shape and offset of the defective SRR as well as to its position in the array.

For the sake of reference, Fig. 7 displays $\mathcal{T}(\mathbf{r})$ through a square surface placed in $x = 0.3\,\text{mm}$ at $f = 100\,\text{GHz}$, in the case when no defects are present in the array. Then, Figs. 8 and 9 show $\mathcal{T}(\mathbf{r})$ as a function of frequency in $\mathbf{r} = (0.3, 1.5, 1.8)\,\text{mm}$ and $\mathbf{r} = (0.3, 2.3, 2.5)\,\text{mm}$, respectively, i.e., right in front of the corresponding defective SRRs. Finally, Figs. 10 and 11 show cuts of $\mathcal{T}(\mathbf{r})$ along the straight lines highlighted in Fig. 7. In Figs. 8–11, the parameter of the lines is the label assigned to the regular and the defective SRRs in Fig. 6.

On comparing the plots, we see, for instance, that the transmission efficiency is most affected when the defective SRR possesses a different size [cases (e) and (f)] — which is more apparent when the defect occurs closer to the source (Fig. 8). On the other hand, the transmission efficiency appears more sensitive to the offset of one SRR [cases (b)–(d)] when the defect is located farther away from the source (Fig. 9).

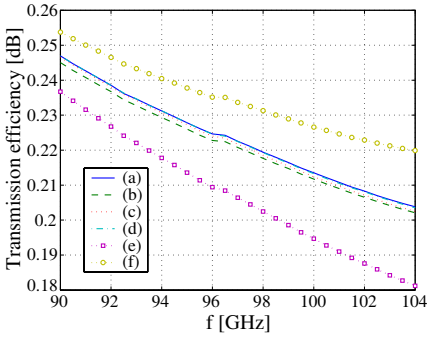

Figure 8. Transmission efficiency (24) of the array in Fig. 5 at $\mathbf{r} = (0.3, 1.5, 1.8)\,\text{mm}$ as a function of frequency and relevant to position #1 of the defective SRR. The labels of the lines point to the SRRs displayed in Fig. 6.

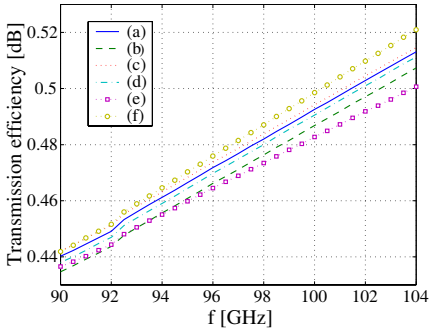

Figure 9. Same as Fig. 8 for $\mathbf{r} = (0.3, 2.3, 2.5)\,\text{mm}$ and relevant to position #2 of the defective SRR.

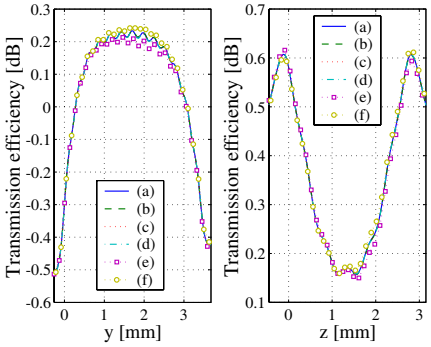

Figure 10. Transmission efficiency (24) of the array in Fig. 5 at $f = 100\,\mathrm{GHz}$ and relevant to position #1 of the defective SRR: (left) along the line $\mathbf{r} = (0.3, y, 1.8)\,\mathrm{mm}$, (right) along the line $\mathbf{r} = (0.3, 1.5, z)\,\mathrm{mm}$. The labels of the lines point to the SRRs displayed in Fig. 6.

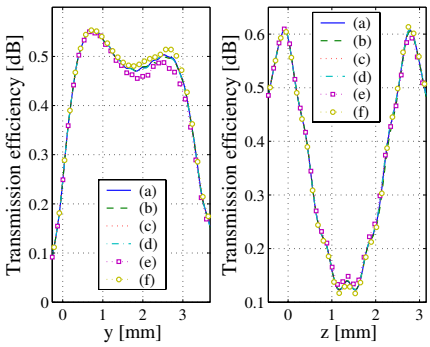

Figure 11. Same as Fig. 10 but relevant to position #2 of the defective SRR: (left) along the line $\mathbf{r} = (0.3, y, 2.5)\,\mathrm{mm}$, (right) along the line $\mathbf{r} = (0.3, 2.3, z)\,\mathrm{mm}$.

5. CONCLUSIONS AND PERSPECTIVES

We have discussed a methodology (based on LEGO and the EEM) for efficiently dealing with large structures comprised of many bodies. We have demonstrated that LEGO/EEM can perform much better than the baseline MoM for a specific class of EM problems — i.e., arrangements of identical bodies plus a different (or defective) one — in that the resulting reduced algebraic system (19) can be solved with direct methods (and multiple right hand sides) rather than with iterative methods. Even though we have used LEGO/EEM to assess the sensitivity of a structure, our approach applies as well for designing or optimizing localized geometry details or EM properties of a large structure, as we did in [21].

Finally, so far LEGO has been applied to aggregates of distinct objects. Nonetheless we are convinced that LEGO has the potential of reducing the complexity of EM problems which involve large homogeneous (e.g., similarly to [14]) and inhomogeneous dielectric bodies: Extension in this direction is ongoing and will be the subject of other papers.

ACKNOWLEDGMENT

This research was supported by the post-doc fund under TU/e project no. 36/363450, and is performed in the framework of the MEMPHIS project (http://www.smartmix-memphis.nl).

REFERENCES

1. Engheta, N., W. D. Murphy, V. Rokhlin, and M. S. Vassiliou, "The fast multipole method (FMM) for electromagnetic problems," *IEEE Trans. Antennas Propag.*, Vol. 40, 634–641, Jun. 1992.
2. Song, J. M., C. C. Lu, and W. C. Chew, "MLFMA for electromagnetic scattering from large complex objects," *IEEE Trans. Antennas Propag.*, Vol. 45, 1488–1493, Oct. 1997.
3. Harrington, R. F., *Field Computation by Moment Methods*, MacMillan, New York, 1968.
4. Peterson, A. F., S. L. Ray, and R. Mittra, *Computational Methods for Electromagnetics*, IEEE Press, Piscataway, 1998.
5. Balanis, C. A., *Advanced Engineering Electromagnetics*, Wiley, New York, 1989.
6. Peng, Z. Q. and A. G. Tijhuis, "Transient scattering by a lossy dielectric cylinder: Marching-on-in-frequency approach," *Journal of Electromagnetic Waves and Applications*, Vol. 7, No. 5, 1993.
7. Tijhuis, A. G., M. C. Beurden, and A. P. M. Van Zwamborn, "Iterative solution of field problems with a varying physical parameter," *Elektrik, Turkish Journal of Electrical Engineering & Computer Sciences*, Vol. 10, No. 2, 2002.
8. Yeo, J., V. V. S. Prakash, and R. Mittra, "Efficient analysis of a class of microstrip antennas using the characteristic basis function method (CBFM)," *Microwave and Optical Technology Letters*, Vol. 39, No. 6, 456–464, 2003.
9. Mittra, R. and K. Du, "Characteristic basis function method for iteration-free solution of large method of moments problems," *Progress In Electromagnetics Research B*, Vol. 6, 307–336, 2008.
10. Li, M. K. and W. C. Chew, "Wave-field interaction with complex structures using equivalence principle algorithm," *IEEE Trans. Antennas Propag.*, Vol. 55, 130–138, Jan. 2007.
11. Matekovitz, L., V. A. Laza, and G. Vecchi, "Analysis of large complex structures with the synthetic-functions approach," *IEEE Trans. Antennas Propag.*, Vol. 55, 2509–2521, Sep. 2007.
12. Yuan, H.-W., S.-X. Gong, Y. Guan, and D.-Y. Su, "Scattering

analysis of the large array antennas using the synthetic basis functions method," *Journal of Electromagnetic Waves and Applications*, Vol. 23, No. 2–3, 309–320, 2009.

13. Ylä-Oijala, P. and M. Taskinen, "Electromagnetic scattering by large and complex structures with surface equivalence principle algorithm," *Waves in Random and Complex Media*, Vol. 19, 105–125, Feb. 2009.
14. Xiao, G., J.-F. Mao, and B. Yuan, "A generalized surface integral equation formulation for analysis of complex electromagnetic systems," *IEEE Trans. Antennas Propag.*, Vol. 57, 701–710, Mar. 2009.
15. Laviada, J., F. Las-Heras, M. R. Pino, and R. Mittra, "Solution of electrically large problems with multilevel characteristic basis functions," *IEEE Trans. Antennas Propag.*, Vol. 57, 3189– 3198, Oct. 2009.
16. Golub, G. H. and C. F. V. Loan, *Matrix Computations*, Johns Hopkins University Press, Baltimore, 1996.
17. Van De Water, A. M., B. P. De Hon, M. C. Van Beurden, A. G. Tijhuis, and P. De Maagt, "Linear embedding via Green's operators: A modeling technique for finite electromagnetic band-gap structures," *Phys. Rev. E*, Vol. 72, 1–11, Nov. 2005.
18. Lancellotti, V., B. P. De Hon, and A. G. Tijhuis, "An eigencurrent approach to the analysis of electrically large 3-D structures using linear embedding via Green's operators," *IEEE Trans. Antennas Propag.*, Vol. 57, 3575–3585, Nov. 2009.
19. Lancellotti, V., B. P. De Hon, and A. G. Tijhuis, "On the convergence of the eigencurrent expansion method applied to linear embedding via Green's operators," submitted Oct. 2009.
20. Bekers, D. J., S. J. L. Van Eijndhoven, and A. G. Tijhuis, "An eigencurrent approach for the analysis of finite antenna arrays," *IEEE Trans. Antennas Propag.*, Vol. 58, Dec. 2009.
21. Lancellotti, V., B. P. De Hon, and A. G. Tijhuis, "A total inverse scattering operator formulation for the analysis of large 3-D structures," *11th ICEAA*, Torino, Italy, Sept. 2009.
22. Lancellotti, V., B. P. De Hon, and A. G. Tijhuis, "Analysis of antennas in the presence of large composite 3-D structures with linear embedding via Green's operators (LEGO) and a modified EFIE," *4th EuCAP*, Barcelona, Spain, to be presented, Apr. 2010.
23. Lindell, I., "Huygens' principle in electromagnetics," *Science, Measurement and Technology, IEE Proceedings*, Vol. 143, 103–105, Mar. 1996.

24. Rao, S. M., D. R. Wilton, and A. W. Glisson, "Electromagnetic scattering by surfaces of arbitrary shape," *IEEE Trans. Antennas Propag.*, Vol. 30, 409–418, May 1982.
25. Anderson, E., Z. Bai, C. Bischof, S. Blackford, J. Demmel, J. Dongarra, J. D. Croz, A. Greenbaum, S. Hammarling, A. McKenney, and D. Sorensen, *LAPACK Users' Guide*, SIAM, 1999.
26. Gürel, L., O. Ergül, and A. Ünal, "Accurate analysis of metamaterials involving finite arrays of split-ring resonators and thin wires," *PIERS Proceedings*, 470–473, Beijing, China, Mar. 26–30, 2007
27. Ergül, O., T. Malas, C. Yavuz, A. Ünal, and L. Gürel, "Computational analysis of complicated metamaterial structures using MLFMA and nested preconditioners," *2nd EuCAP*, Edinburg, UK, Nov. 2007.